Further Numerical Studies of Backscattering From Time-Evolving Nonlinear Sea Surfaces

Alfonso R. Hayslip, Joel. T. Johnson, *Senior Member, IEEE*, and Gregory. R. Baker

***Abstract*—Previous studies have demonstrated that the West *et al.* numerical model for nonlinear hydrodynamic evolution of a sea surface produces significant features in calculated L-band backscattered Doppler spectra compared to a linear sea surface evolution model. These prior comparisons were limited, however, to a maximum wind speed of 2.0 m/s due to failure of the West *et al.* algorithm when steep short-wave features formed on the surface. In this paper, L-band Doppler spectra with the West *et al.* model are reported for wind speeds up to 5.0 m/s through the use of a curvature filter to reduce these steep short waves. The higher wind speed results again show significant deviations from those reported with a linear hydrodynamic model, including increased spectral broadening and polarization dependencies.**

***Index Terms*—Doppler spectrum, rough surface scattering, ocean remote sensing.**

I. Introduction

BACKSCATTERED radar returns from a time-varying ocean surface are distributed into a spectrum through the Doppler effect; this phenomenon has important implications for many remote sensing systems. Scattering predictions based on the first-order small perturbation method and a linear model of the sea surface produce a single Doppler frequency component at the temporal frequency of the Bragg wave in the surface spectrum. Measured microwave Doppler spectra, however, show more features than a single Bragg line, and also exhibit complex incidence angle and polarization dependencies. More realistic models for backscattered Doppler spectra require both more accurate electromagnetic scattering models and more accurate simulations of ocean surface dynamics, which are inherently nonlinear.

Combined numerical hydrodynamic and electromagnetic Monte Carlo simulations with one-dimensional (1-D) surfaces [1], [2] have recently demonstrated a significant influence of nonlinear hydrodynamics on L-band backscattering. Johnson *et al.* [2] employed the West *et al*. hydrodynamic model [3], and demonstrated strong Doppler spectrum broadening compared to a linear model and to the Creamer *et al*. model [4]. Additional results included some evidence of reverse traveling features in the sea surface, and a nonlinear distortion of the surface profile in both horizontal and vertical directions. The West *et al.* model, however, was also found to suffer from instabilities at wind speeds greater than about 2.0 m/s in these simulations, due to the formation of steep short waves that invalidate the use of the slope expansion implicit within the algorithm. An alternative nonlinear hydrodynamic model not considered here is based on the Zakharov equation explored in [5].

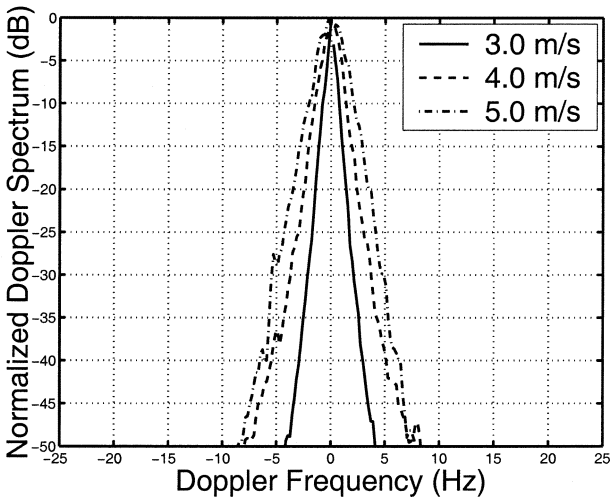

Fig. 1. Doppler spectra for normal incidence (VV polarization shown).

In this paper, further coupled hydrodynamic and electromagnetic simulations are described that extend the previous results up to wind speed 5.0 m/s. This is accomplished through the inclusion of a curvature filter in the West *et al.* model. Although the maximum wind speed of 5 m/s considered here remains somewhat less than the global oceanic average of 7 m/s, the results obtained provide information beyond the previous 2-m/s cases. The basic hydrodynamic algorithm and curvature filter are discussed in the next section, and Section III presents Doppler spectra for wind speeds 3.0, 4.0, and 5.0 m/s at incident angles of 0°, 40°, and 80°. The influence of the curvature filter is examined in Section IV. The data will make it clear that the scattering mechanisms for vertical (VV) and horizontal (HH) polarizations are dissimilar, with horizontal polarization showing a larger mean Doppler shift than vertical polarization. Section V will provide evidence that points to a possible source for these "fast-scatterers."

II. Methodology

The motion of a 1-D irrotational incompressible fluid surface is governed by a pair of nonlinear boundary conditions given in

Manuscript received September 10, 2002; revised March 24, 2003. This work was supported by the Office of Naval Research under Contract N00014-00-1-0399 and by the National Science Foundation under Grant DMS-0112759, and the Maui High Performance Computing Center (MHPCC), which provided the use of the IBM SP parallel computer.

A. R. Hayslip is with Northrop-Grumman, Linthicum, MD 21090 USA.

J. T. Johnson is with the Department of Electrical Engineering and Electro-Science Laboratory, The Ohio State University, Columbus, OH 43210 USA.

G. R. Baker is with the Department of Mathematics, The Ohio State University, Columbus, OH 43210 USA.

Digital Object Identifier 10.1109/TGRS.2003.814662

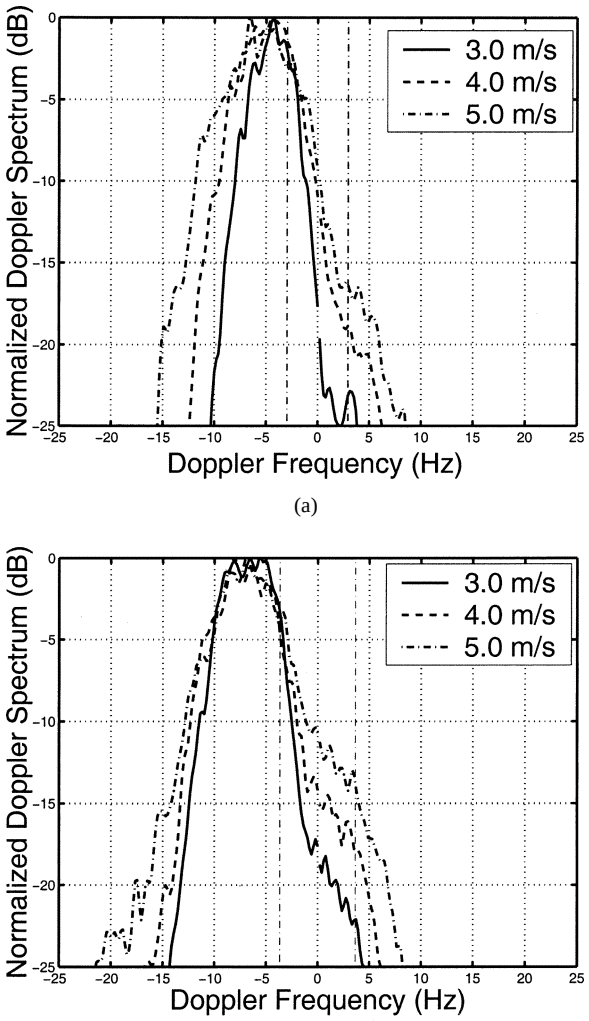

Fig. 2. Doppler spectra for HH polarization (a) 40° and (b) 80°.

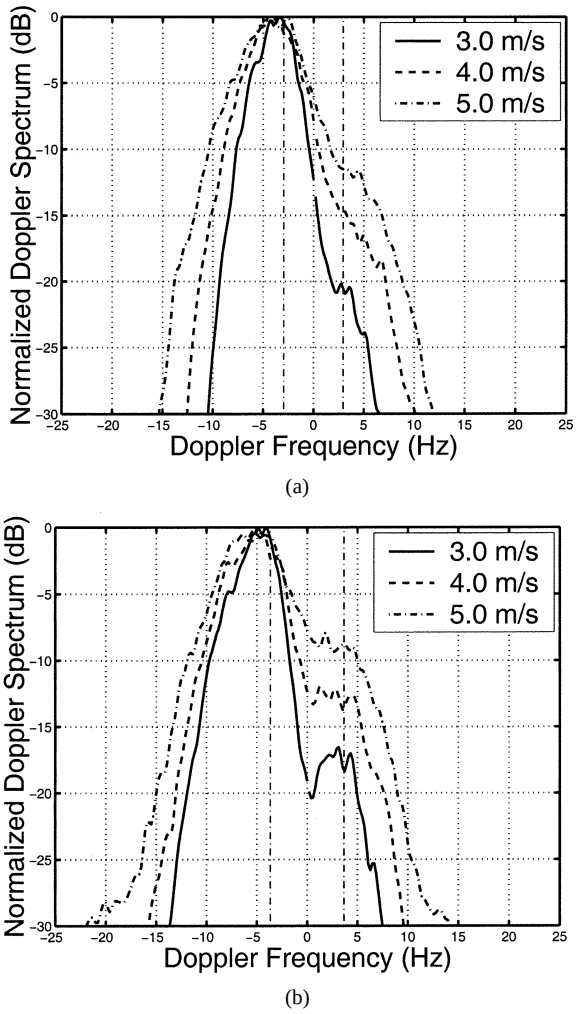

Fig. 3. Doppler spectra for VV polarization (a) 40° and (b) 80°.

[2]. Note that effects due to viscosity and surface tension are not included herein. For a given initial condition, an exact solution to these equations is unknown, making a numerical solution in the form of a time-stepping process necessary to determine the time evolution for h, the surface profile, and ϕ, the velocity potential on the surface. The primary difficulty in this process is evaluating the $\partial\phi/\partial z$ term, since ϕ is only known on the surface. The West method addresses this problem with a perturbation series for the vertical velocity component $\partial\phi/\partial z$. The resulting expansion is in terms of surface slope, and therefore experiences poor convergence in regions where local slopes become large. This approach is advantageous in that through the use of the fast Fourier transform (FFT) the computational demands are reasonable, $O(N \log N)$, where N is the number of surface points. Implied in this model is the use of a fixed, uniformly spaced periodic grid, which prevents the capturing of overturning surface features. However, the model can still produce very steep slopes in some cases. Retaining only the first two terms in the slope series for these intervals will give unacceptable errors that will cause the breakdown of the model. Therefore, the responsibility of the curvature filter will be to ensure that the slope expansion stays within regions of rapid convergence.

Methods for suppressing breaking waves in numerical models have been considered in the literature. Subramani *et al.* [6] proposes a local curvature threshold as a means of detecting potential problematic surface points to improve stability of Stokes wave simulations. This approach is adapted here by calculating the local curvature $\kappa(x)$ at each surface point, and then by scaling $\kappa(x)$ by a, the maximum amplitude of the surface profile at the time step considered. The multiplication of $\kappa(x)$ by a is intended as a means to introduce dependence on the surface profile's height when tagging problematic surface points. For a 1-D surface $h(x)$, $\kappa(x)$ can be written as

$$\kappa(x) = \frac{|h''(x)|}{\left[1 + (h'(x))^2\right]^{3/2}} \tag{1}$$

where $'$ indicates differentiation with respect to x (implemented spectrally in the developed code). The threshold value $(\kappa a)_{\max}$ is a parameter of the detector. Observations of several surface profile simulations described in Section IV showed a value of 16 to be an effective indicator of points that would likely cause the time evolution to fail at future time steps. To suppress problems associated with these points, an interval of $\pm Q$ points centered at each detected point is removed from both the surface profile h and velocity potential ϕ. The union of these deleted

TABLE I
AVERAGE NORMALIZED RADAR CROSS SECTIONS FOR VARYING WIND SPEEDS

Incidence ∠	pol.	RCS (dB) 2.0m/s	RCS (dB) 3.0m/s	RCS (dB) 4.0m/s	RCS (dB) 5.0 m/s
0	VV	15.83	2.463	1.284	1.045
40	VV	−22.91	−22.61	−22.40	−22.77
80	VV	−31.25	−30.71	−30.14	−30.66
0	HH	15.81	2.594	1.411	1.164
40	HH	−28.63	−27.79	−27.786	−28.29
80	HH	−56.43	−53.03	−50.891	−50.88

neighborhoods are replaced by spline interpolated values using the remaining surface profile and velocity potential points, respectively. The value Q is another parameter of the filter; tests with several profiles for the simulations described in Section III showed a value of three points to be sufficient in preventing numerical breakdown. Note that the oversampling requirement implicit in the West *et al.* method reduces the filter's influence for small Q values. The above procedure is applied at the conclusion of each time step.

III. RESULTS

The governing hydrodynamic partial differential equations are initialized with a realization of a Pierson–Moskowitz (P–M) spectrum (as in [1] and [2]) and then advanced in time using a fourth-order Adams–Bashforth predictor-corrector scheme. Notice that the wind speed enters into the model only through the initial surface wave spectrum: no wind forcing terms are included in the simulation. An adjustment period is included in order to gradually turn on the nonlinear terms to avoid a mismatch of initial conditions, since the initial $\phi(x, t = 0)$ is obtained linearly from $h(x, t = 0)$ [7]. This "ramp-up" scheme multiplies the nonlinear terms appearing in the hydrodynamic equations by

$$R(t) = 1 - e^{-(t/T_a)^2} \tag{2}$$

where t denotes time in seconds, and T_a is the period of adjustment. The length of the adjustment period used is $T_o = 3.94$ s (i.e., $T_a = 1.5$ s such that $R(T_o) = 0.999$), and only afterward do the electromagnetic scattering computations begin. Terms up to fourth-order in the Watson–West expansion are included, and to limit spectral content a spatial high-frequency cut-off of $k_h = 109$ rads/m is used (as in [2]). Electromagnetic scattering calculations again use the two-dimensional method of moments numerical procedure described in [2] to compute L-band (23-cm wavelength) backscattering under "tapered beam" illumination with an impedance boundary condition model of the sea water.

Backscattered field Doppler spectra are then computed at wind speeds 3.0, 4.0, and 5.0 m/s, and for observation angles of 0°, 40°, and 80° from normal incidence. The same 117.81-m surface, discretized into 16 384 points, is used for all angles to avoid diffraction effects at the largest observation angle and to avoid hydrodynamic aliasing problems in the Bragg spectral region. Doppler spectra are computed from 256 backscattered field time samples spaced in intervals of 20 ms. This is performed for an ensemble of 64 distinct surface realizations. By using the computing resources at the Maui High Performance Computing Center, Maui, HI (www.mhpcc.edu), the Monte Carlo simulation is accomplished in parallel by running each surface realization on a separate node of the system.

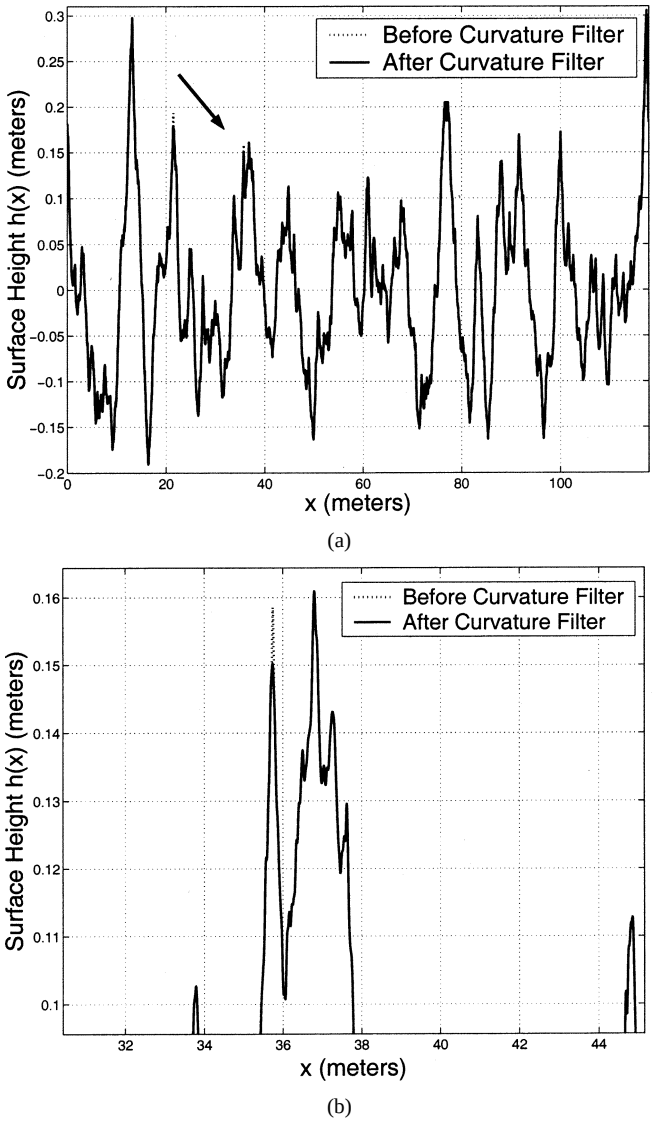

Fig. 4. Surface profile (4 m/s) before and after application of curvature filter. (a) Entire profile. (b) Partial profile.

Results in Figs. 1–3 for 0°, 40°, and 80° show Doppler spectra that are broader than those observed in the previous 2.0-m/s wind speed study [2]; note the Bragg frequencies marked by the dashed–dotted lines. For normal incidence, the results are shown in Fig. 1 for increasing wind speeds. The scattering at this angle is dominated by specular reflection, and no polarization influence is seen. The bandwidth of the spectra does vary, however, and is proportionate to the wind speed.

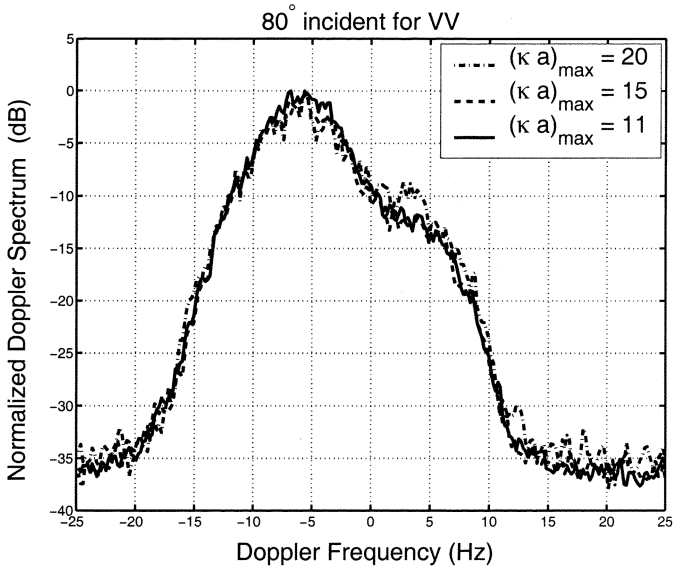

Fig. 5. Calculated Doppler spectra for different values of $(\kappa a)_{\max}$.

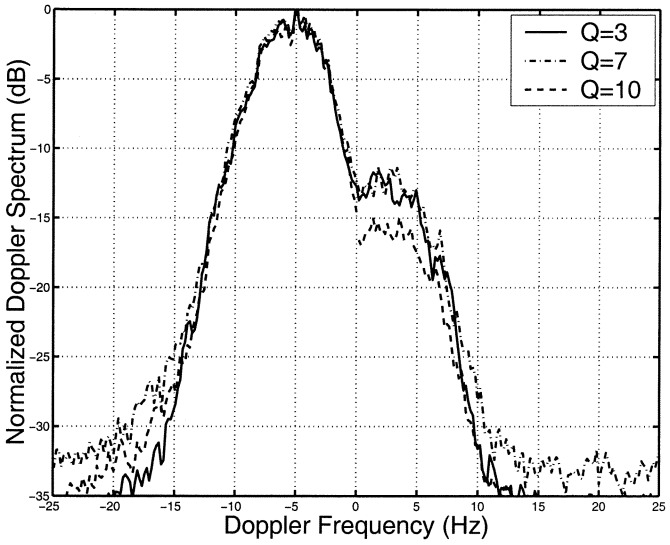

Fig. 6. Calculated Doppler spectra for different values of Q (VV pol. at 80° incidence shown).

Figs. 2 and 3 consider the 40° and 80° cases for both polarizations. For these angles, stronger evidence of reverse traveling features (i.e., the plateau at positive Doppler frequencies) in the surface is evident as the wind speed is increased, especially for the VV spectra. The spectrum shown in Fig. 2(b) possesses slightly greater bandwidth, and stronger positive frequency content when compared to the result obtained in [1] for 5 m/s at 80° incidence using the Creamer *et al.* hydrodynamic model. The adjustment period parameter T_a was varied in order to ensure that the resultant Doppler spectra were not being affected. It was found that T_a had almost no influence on the Doppler spectrum, and this is suggestive that the features present in the spectra such as reverse traveling waves are not generated by the initial conditions.

Table I displays the average normalized radar cross sections (RCS) for increasing wind speeds for both VV and HH polarizations. The data shows the RCS at 5 m/s to be within a decibel of the result for the 4.0-m/s case at 40° and 80° incidence. Comparing the RCS for HH at 80° against the different wind speeds, it is revealed that from 2.0–3.0 m/s the RCS increases by more than 3 dB, and then increases by just over 2 dB as the wind speed grows to 4.0 m/s. This observed saturation of the RCS is found to be similar to the predictions of two-scale theory. For comparison, the two-scale theory with the initial P–M spectrum reports for 80° incidence and wind speeds of 4 and 5 m/s RCS values of −54.7 and −54.1 dB respectively for the HH case, and −31.71 and −31.66 dB for VV.

IV. Filter Issues

To investigate the hydrodynamic effects of the curvature filter several Monte Carlo simulations were performed with the filter in place in order to determine its influence on such quantities as Doppler spectra, surface profile, etc. Fig. 4 illustrates a sample surface realization before and after the curvature filter is applied, and shows the suppression of steep short-wave features achieved by the filter. It is clear that the filter is modifying the surface profile $h(x,t)$ so that these simulations can be continued. These steep waves, however, comprise a relatively small percentage of the sea surface, as Fig. 4 exemplifies. Assessing the influence of this filter on surface hydrodynamic evolution is difficult given the complexity of the nonlinear equations. Of course, it is desirable to minimize the influence so that no strong nonphysical effects are introduced. Doppler spectra results varying the values of $(\kappa a)_{\max}$ and Q can be used to provide some insight into filter influence. Figs. 5 and 6 show that as the filter is turned off, i.e., as $Q \to 0$ and $(\kappa a)_{\max} \to \infty$, the resultant VV Doppler spectra at 80° incidence show only minor variations. When $(\kappa a)_{\max} = 20$, more nonlinear effects and reverse waves are observed in the Doppler spectra, while for $Q = 10$ these features become more subdued. It is also apparent that the value of Q has a slightly greater influence on the reverse wave part of the spectrum than does the threshold level. These Doppler spectra are obtained via Monte Carlo simulations as described in Section III.

TABLE II
Filter Operation Statistics for 64 Realizations With Each Profile Consisting of 16 384 Points

Wind Speed (m/s)	2.1	3.0	4.0	5.0
% of time steps filter activated	.093	4.44	30.0	57.23
Mean # of points deleted upon activation	7.00	7.63	15.3	19.2

Statistics on the number of points modified and the frequency of filter operations can also provide some information. Table II reveals the extent of the filter's modification to the surface. This data was compiled using $Q = 3$, $(\kappa a)_{\max} = 11$, and with 16 384 points per profile. The 3-m/s case shows that the filter is required significantly less than for the higher wind speed surfaces where unstable structures are more likely to form on the surface. For wind speeds under about 2 m/s, the hydrodynamic code is stable, and no filtering is necessary. For a limiting case using wind speed of 2.1 m/s, the curvature filter seldom activates, and when it does only the minimum number of points are interpolated. Even though the number of points being modified increases with wind speed, their relatively small values

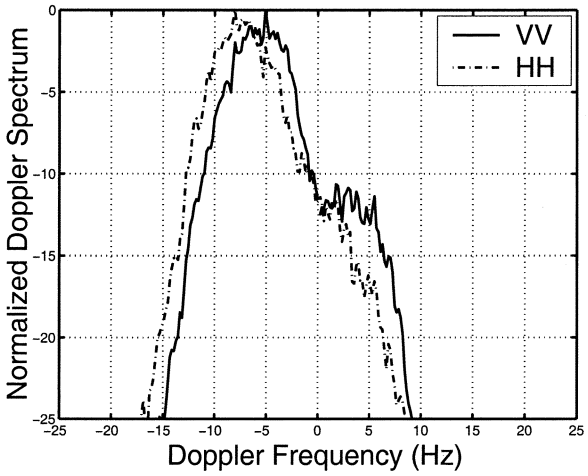

Fig. 7. Comparison of averaged Doppler spectra for ensemble of 128 realizations.

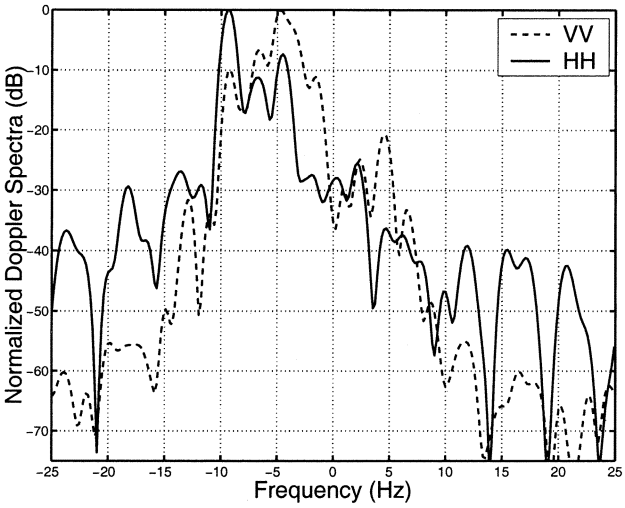

Fig. 8. Single realization Doppler spectrum with a strong polarization influence.

(e.g., at worst case an average of 0.12% of the surface points are modified per time step) suggest that the overall influence of the filter on the Doppler spectrum may only be minor. It is important to note, however, that this simulation does not capture overturning waves. Therefore, any possible contributions to the Doppler spectrum due to these features are not included.

V. "Fast Scatterers"

Polarization dependencies become observable as the incident angle is tilted away from normal, with HH showing a larger mean Doppler shift than VV. Fig. 7 illustrates this for 80° incidence at 5.0 m/s. These results appear to capture some of the "fast-scatterering" phenomena observed in measured sea backscattering data. More insight concerning the sources of these "fast scatterers" can be gained by considering the backscatter from just a single realization. Fig. 8 is a plot of a single realization Doppler spectrum showing a large polarization difference. The non-Bragg scattering mechanisms responsible for this effect, unlike Bragg scattering, are thought to be localized in space and time (e.g., see [8]).

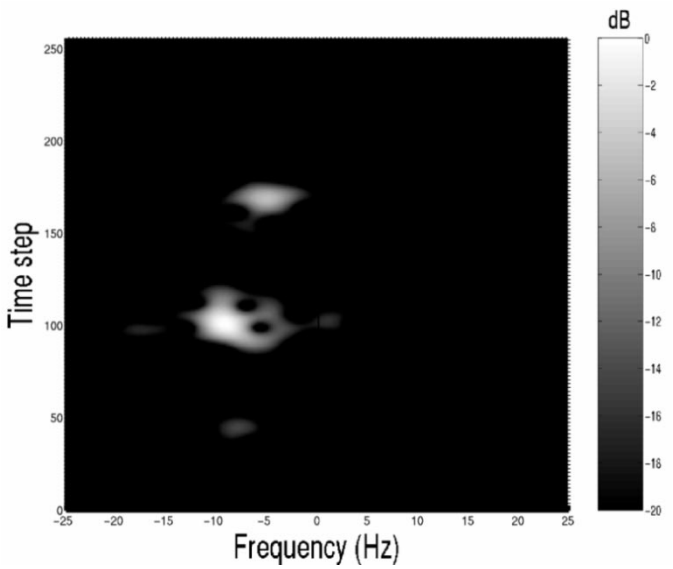

Fig. 9. Plot of normalized local Doppler spectrum.

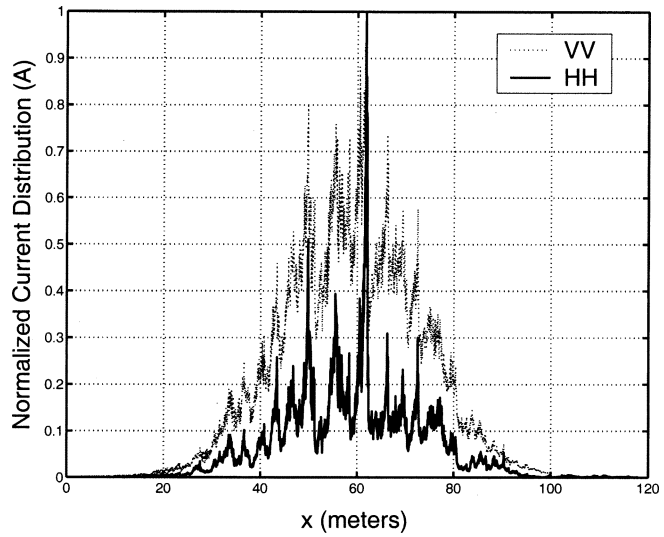

Fig. 10. Currents induced on profile at time 5.34 s; note peak for HH at 62 m.

To begin testing this idea, the local HH Doppler spectrum is computed for each time step. This was accomplished by passing the scattered field data through a Gaussian window, whose peak is centered at the time step currently being considered, before computing the Doppler spectrum. The 3-dB bandwidth of the Gaussian window is six time samples. In Fig. 9 the normalized HH local Doppler spectrum is plotted as a function of both time and frequency. As was seen in Fig. 8 the peak for the HH spectrum is at $f \approx -9.33$ rads/s, and now looking at Fig. 9 for the same f a relative maximum is observed at time step 110 (i.e., at $\approx$ 5.34 s). This region indicates an interval of time where the contribution to this peak is significant, and in order to pinpoint where on this surface the scattering center is, the electric currents induced on the profile for both polarizations are examined. In Fig. 10, the peak at $\approx$ 62 m for both VV and HH is readily apparent. For the HH case, this maximum is the dominant feature in the plot. For VV the peak is still visible, but is accompanied by the stronger Bragg response. Upon exami-

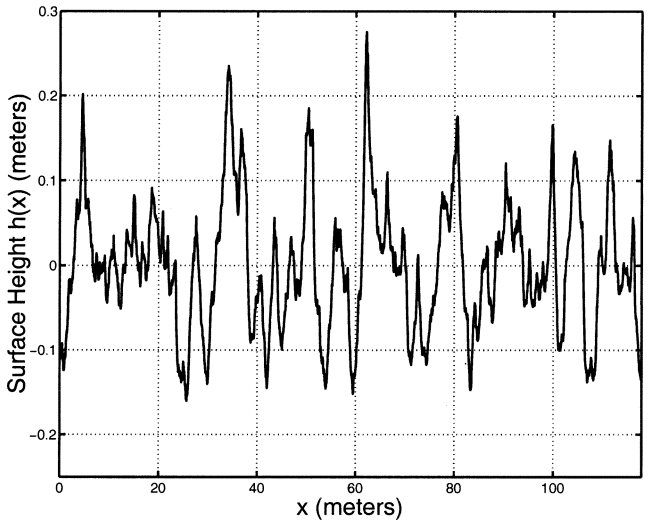

Fig. 11. Profile at 5.34 s during time evolution of Fig. 8.

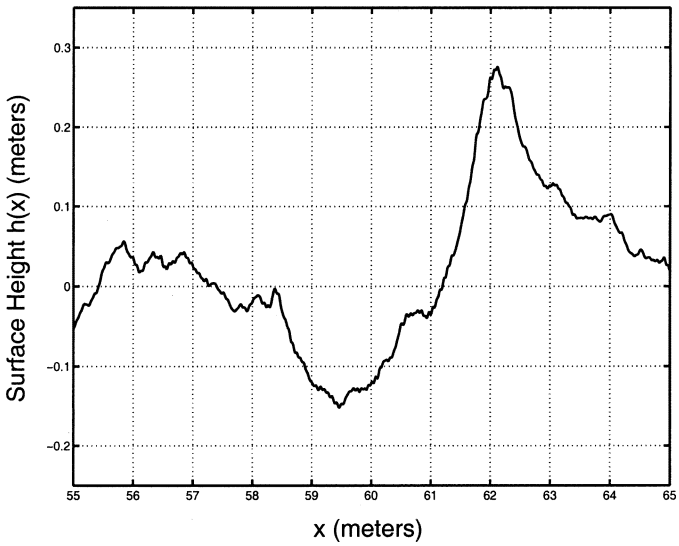

Fig. 13. Expanded view of the profile in Fig. 11.

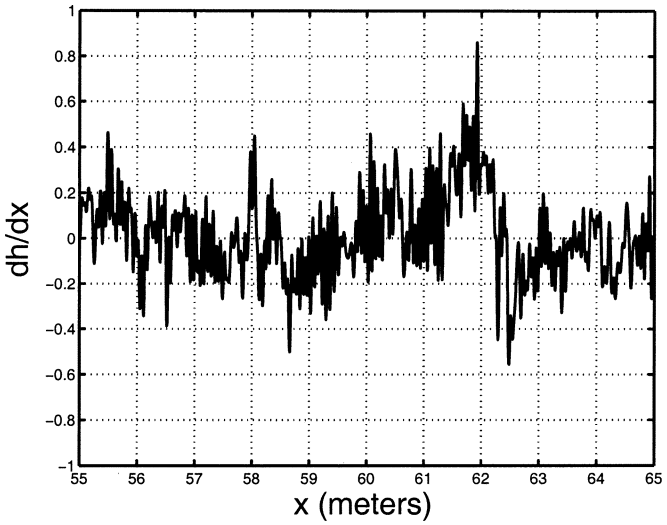

Fig. 12. Corresponding slope of the partial profile in Fig. 13.

nation of the corresponding surface profile shown in Fig. 11, $h(x = 62\ \text{m}, t = 5.12\ \text{s})$, a large steep slope is observed, which suggests that this feature is part of the cause for the peak differences in the two polarizations for this particular realization. Additionally, by examining Fig. 12, the surface slope is revealed in a neighborhood about the peak, and it is seen to be not sufficient for near specular reflection. The corresponding profile segment is shown in Fig. 13.

VI. Conclusion

This paper has presented P–M initialized Doppler spectra for wind speeds greater than 2.0 m/s using the West *et al.* nonlinear hydrodynamic model with a curvature filter in order to stabilize the model for higher wind speeds. This filter is needed in order to make these large-scale studies possible. Data acquired through extensive tests concerning the filter suggest the filter's influence on the Doppler spectrum is minimal in these results, although a complete conclusion in this regard is not possible due to the instability of the hydrodynamic algorithm. The West *et al.* model has been shown to capture a larger amount of nonlinear interactions [2] such as profile distortion, reverse traveling waves, etc. At higher wind speeds, these nonlinear interactions were shown to become more pronounced. In particular, polarization differences at low grazing angles were observed. Moreover, some evidence for identifying a possible source of this effect was presented from the numerical data for a specific case. These results work to increase understanding of sea surface electromagnetic scattering and will aid in improving sea-based remote sensing systems.

References

[1] J. V. Toporkov and G. S. Brown, "Numerical simulations of scattering from time-varying, randomly rough surfaces," *IEEE Trans. Geosci. Remote Sensing*, vol. 38, pp. 1616–1624, July 2000.

[2] J. T. Johnson, J. V. Toporkov, and G. S. Brown, "A numerical study of backscattering from time-evolving sea surfaces: Comparison of hydrodynamic models," *IEEE Trans. Geosci. Remote Sensing*, vol. 39, pp. 2411–2419, Nov. 2001.

[3] B. J. West, K. Brueckner, R. Janda, D. Milder, and R. Milton, "A new numerical method for surface hydrodynamics," *J. Geophys. Res.*, vol. 92, pp. 11 803–11 824, 1987.

[4] D. B. Creamer, F. Henyey, R. Schult, and J. Wright, "Improved linear representation of ocean surface waves," *J. Fluid Mech.*, vol. 205, pp. 135–161, 1989.

[5] S. Y. Annenkov and V. Shrira, "Numerical modeling of water-wave evolution based on the Zakharov equation," *J. Fluid Mech.*, vol. 449, pp. 341–371, 2001.

[6] D. Dommermuth, "The initialization of nonlinear waves using an adjustment scheme," *Wave Motion*, vol. 32, pp. 307–317, 2000.

[7] D. Dommermuth, "The initialization of nonlinear waves using an adjustment scheme," *Wave Motion*, vol. 32, pp. 307–317, 2000.

[8] A. N. Churyumov and Y. A. Kravtsov, "Microwave backscatter from mesoscale breaking waves on the sea surface," *Waves Random Media*, vol. 10, pp. 1–15, 2000.

Alfonso R. Hayslip received the B.S. degree from the University of Dayton, Dayton, OH, and the M.S. degree from The Ohio State University, Columbus, in 2001 and 2003, respectively, both in in electrical engineering.

He is currently a Systems Engineer with Northrop-Grumman Corporation, Lithicum, MD.

Joel T. Johnson (S'91–M'96–SM'03) received the B.E.E. degree from the Georgia Institute of Technology, Atlanta, in 1991, and the S.M. and Ph.D. degrees from the Massachusetts Institute of Technology, Cambridge, in 1993 and 1996, respectively.

He is currently an Associate Professor in the Department of Electrical Engineering and ElectroScience Laboratory, The Ohio State University, Columbus. His research interests are in the areas of microwave remote sensing, propagation, and electromagnetic wave theory.

Dr. Johnson is a member of International Union of Radio Science (URSI) Commissions B and F, as well as a member of Tau Beta Pi, Eta Kappa Nu, and Phi Kappa Phi. He has received the 1993 Best Paper Award from the IEEE Geoscience and Remote Sensing Society, was named an Office of Naval Research Young Investigator, National Science Foundation Career awardee, and PECASE Award recipient in 1997, and was recognized by the U.S. National Committee of URSI as a Booker Fellow in 2002.

Gregory R. Baker received the Ph.D. degree from the California Institute of Technology, Pasadena, in 1997.

He has been an Assistant Professor with the Massachusetts Institute of Technology, Cambridge; a Full Professor and Director of the Applied Mathematics Program at the University of Arizona, Tucson; a Research Mathematician at the Exxon Research and Engineering Company; and The Ohio Eminent Scholar in Scientific Computation at The Ohio State University, Columbus, where he is currently a member of the Department of Mathematics. His research include the numerical solution of partial differential equations with a specialization in moving boundary problems.

Dr. Baker was one of the first Presidential Young Investigators (awarded in 1984). He is a member of the American Physical Society.